Electronic Supplementary Information

Targeted Design Strategies for Highly Activated Carbon Cloth Cathode/Anode to Construct Flexible and Cuttable Sodium Ion Capacitors with All-Woven-Structure

Ying-Ying Wang,[ab] Zhong-Yuan Wang,[b] Yu-Juan Xu,[b] Wei-Hua Chen,[c] Guo-Sheng Shao*[a] and Bao-Hua Hou*[a]*

[a] State Centre for International Cooperation on Designer Low-Carbon & Environmental Materials, School of Materials Science and Engineering, Zhengzhou University, Zhengzhou 450001, P. R. China.

E-mail: houbh019@zzu.edu.cn

[b] Henan Institute of Advanced Technology, Zhengzhou University, Zhengzhou 450001, P. R. China.

[c] College of Chemistry, Zhengzhou University, Zhengzhou 450001, P. R. China.

Experimental Section

Preparation of HCC: Briefly, the cotton cloth was firstly heated in the air at 240 °C for 8 h with a heating rate of 3 °C min^{-1}, obtaining the pre-oxidation carbonaceous cotton cloth (POCC) as the furnace was cooled to room temperature. Specifically, pre-oxidation process can serve to stabilize the structure, reduce shrinkage, and increase residual carbon. Meanwhile, it is helpful to reduce defects and improve the initial coulombic efficiency of the anode. Subsequently, such POCC was further annealed in the Ar at 1300 °C for 3 h with the same heating rate of 3 °C min^{-1}. After being cooled naturally to room temperature, the HCC could be collected easily. The residual carbon rate and the areal density of HCC are 19% and ≈4 mg cm^{-2}, respectively.

Preparation of PCC: The cotton cloth was firstly heated in the Ar at 400 °C for 3 h with a heating rate of 5 °C min^{-1}, obtaining the pre-carbonization carbonaceous cotton cloth (PCCC) as the furnace was cooled to room temperature. Specifically, pre-carbonization can also serve to stabilize the structure, reduce shrinkage, and increase residual carbon. Next, KOH aqueous solution (1 mL, 2 mol L^{-1}) is slowly added dropwise to PCCC (2 cm*8 cm) until PCCC is evenly infiltrated. After drying in the vacuum at 60 °C for 10 h, the PCCC was further annealed

in the Ar at 800 °C for 4 h with the heating rate of 5 °C min^{-1}. After being cooled naturally to room temperature, the obtained product was washed with 1 mol L^{-1} HCl solution and distilled water, next dried at 60 °C for 10 h in a vacuum. The PCC could be obtained. The residual carbon rate and the areal density of HCC are 12% and ≈2 mg cm^{-2}, respectively.

Structural and morphological characterization: The morphology of the materials was recorded by scanning electron microscopy (SEM, ZEISS GeminiSEM 300) and transmission electron microscopy (TEM, FEI Talos F200X microscope, 200 kV). Powder X-ray diffraction (XRD) patterns were tested using Cu Kα radiation (λ=1.5405 Å) on the Rigaku SmartLab SE. Raman spectroscopy was performed on a LabRAM HR Evolution instrument at an excitation wavelength of 532 nm. X-ray photoelectron spectrometer (XPS) data were collected by ThermoFischer Escalab 250 Xi with an Al Kα X-ray source（hv=1486.6 eV）.The surface area and porous structure were analyzed using Micromeritics ASAP 2460 instrument according to the N_2 adsorption-desorption isotherms.

Electrochemical Measurements: Electrochemical performances of the samples were tested in the coin-type cells of CR2032, which were assembled in the Ar-filled glovebox. All the half-cells were constructed with the sodium foils as the counter electrode. The working electrodes were flexible HCC or PCC, which were directly used as the self-supporting electrodes without any treatment. 1.0 mol L^{-1} $NaPF_6$ in methoxymethane (abbreviated as 1M $NaPF_6$/DME) or 1.0 mol L^{-1} $NaClO_4$ in propylene carbonate with 5 wt% fluoroethylene carbonate (abbreviated as 1M $NaClO_4$/[PC+5%FEC]) was used as the electrolyte solution. Glass fiber (GF/D) from Whatman was used as a separator.

All electrochemical properties were tested in a thermostat at 25 °C. GCD tests were carried out on the Neware battery testing devices (CT-4008T) in the potential window of 1.0-4.0 V and 0.01-2.8 V vs. Na^+/Na for half cells. CV tests were performed on a CHI 760E electrochemical station in the same potential window. Electrochemical impedance spectroscopy (EIS) was tested on a Biologic EC Lab VMP-3 electrochemical station. The ACSIC (CR2032 coin-type cells and flexible pouch cells) was fabricated using HCC as the anode and PCC as the cathode. Their electrochemical properties were evaluated in the voltage window of 1.0-3.8 V. Prior to the fabrication of ACSIC, chemical presodiation for the HCC anode was performed to activate the material and stabilize the electrode surface. In the pre-sodiation processes, electrolyte was added on the anodes which were contacted with the metallic sodium. The pre-sodiation times is about 30 min.

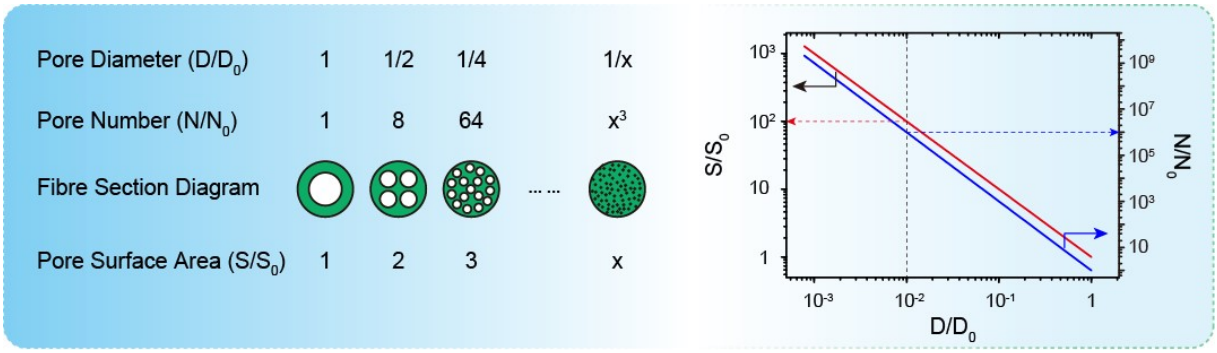

Fig. S1. Assuming that the total pore volume is the constant, correspondence of pore number vs. pore diameter and specific surface area vs. pore diameter.

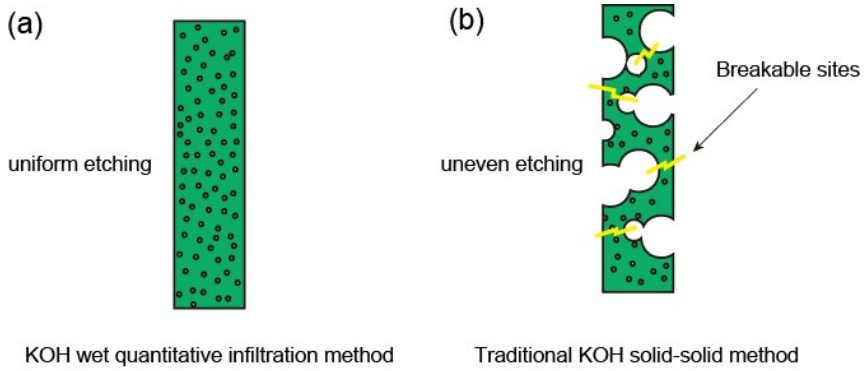

Fig. S2. Structural schematic of PCC prepared by (a) KOH wet quantitative infiltration method and (b) traditional KOH solid-solid method.

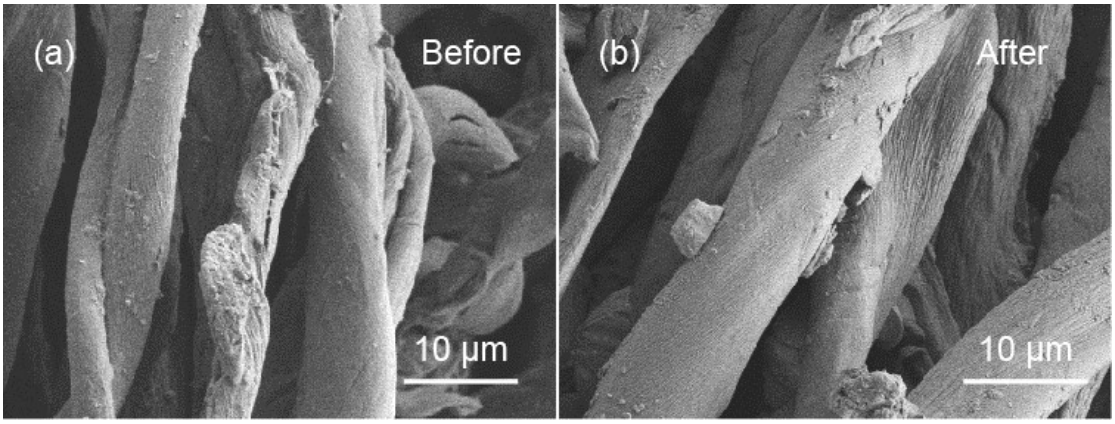

Fig. S3. SEM images of PCCC (a) before and (b) after KOH wet quantitative infiltration.

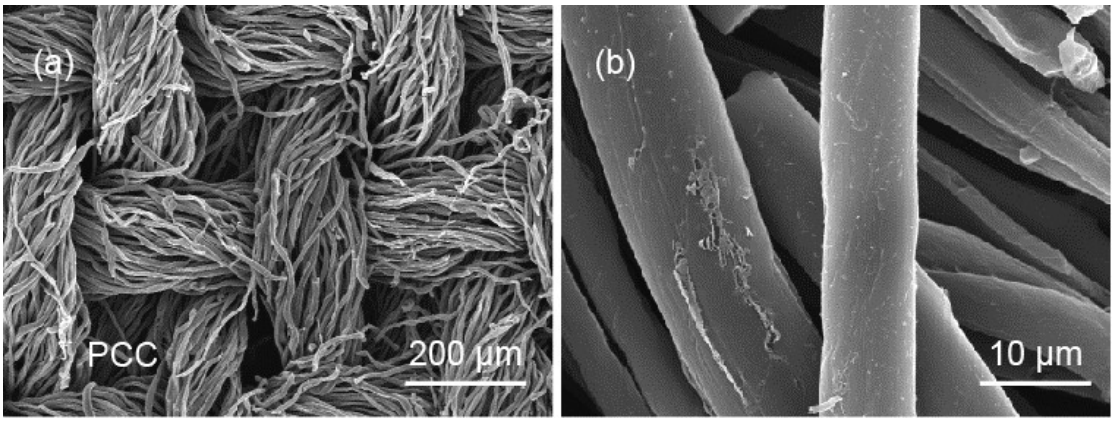

Fig. S4. SEM images of PCC.

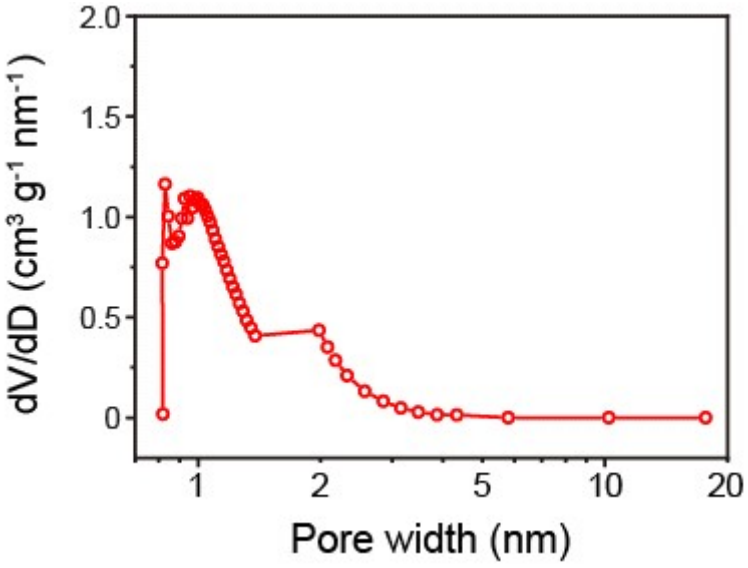

Fig. S5. The BJH pore size distribution of PCC.

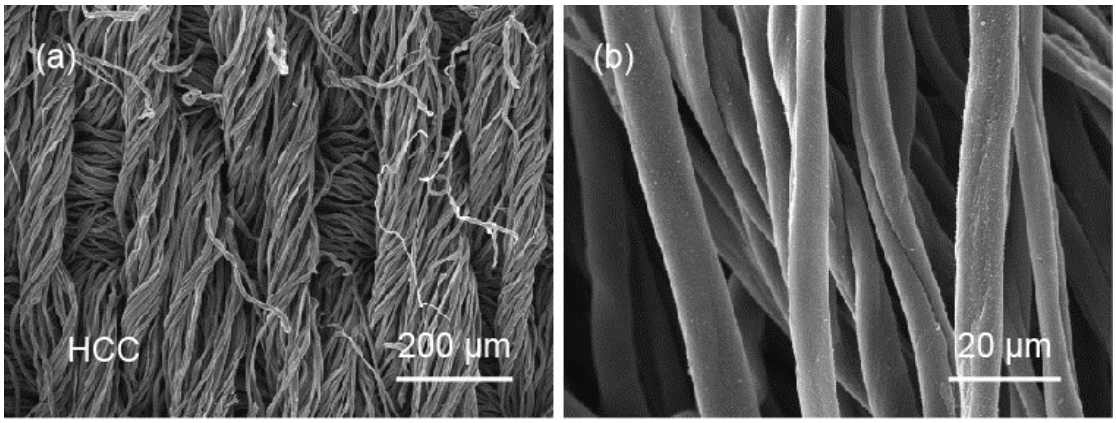

Fig. S6. SEM images of HCC.

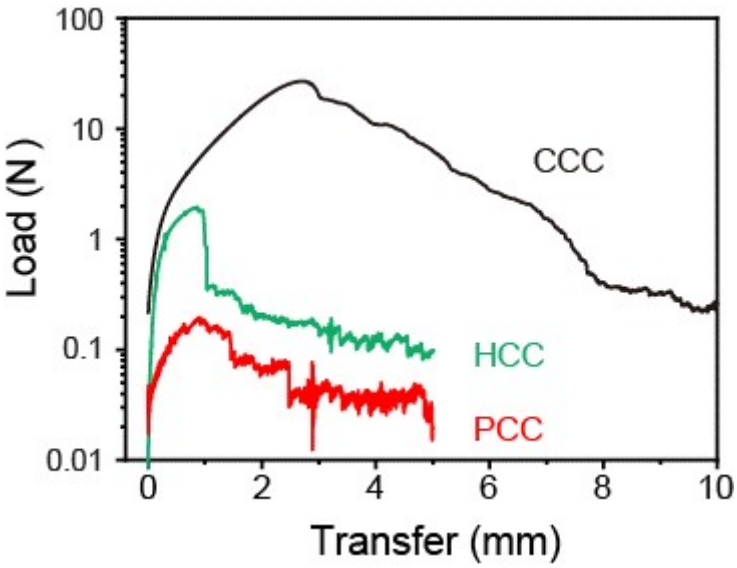

Fig. S7. Variation of load with migration distance PCC, HCC, and CCC.

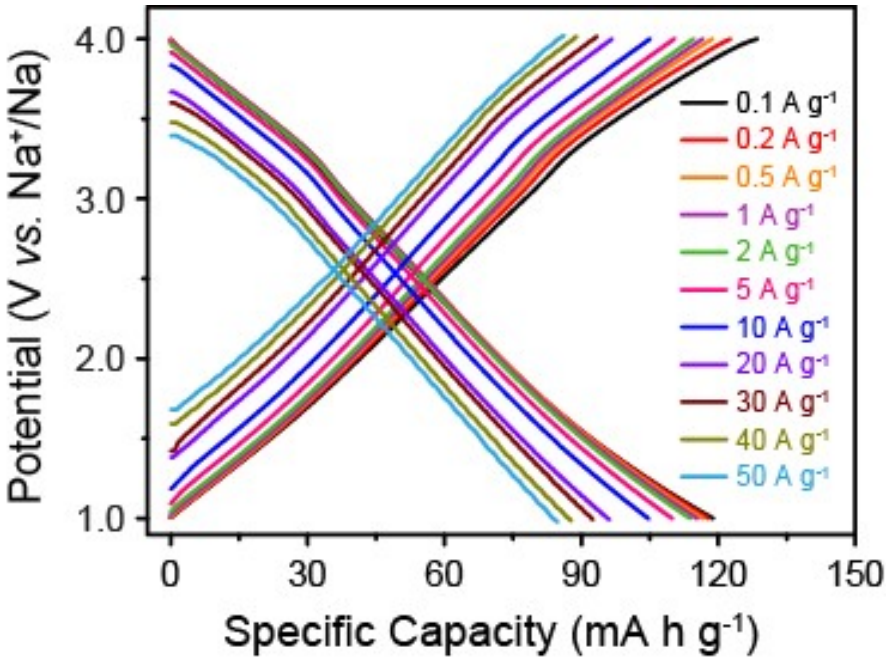

Fig. S8. GCD curves of PCC cathode at different J.

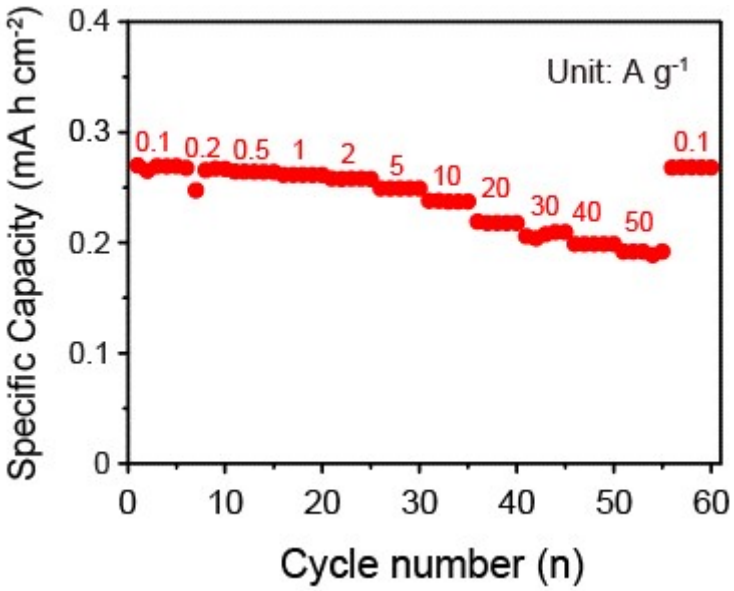

Fig. S9. Rate capability of PCC cathode at various J from 0.1 to 50 A g^{-1} calculated based on area.

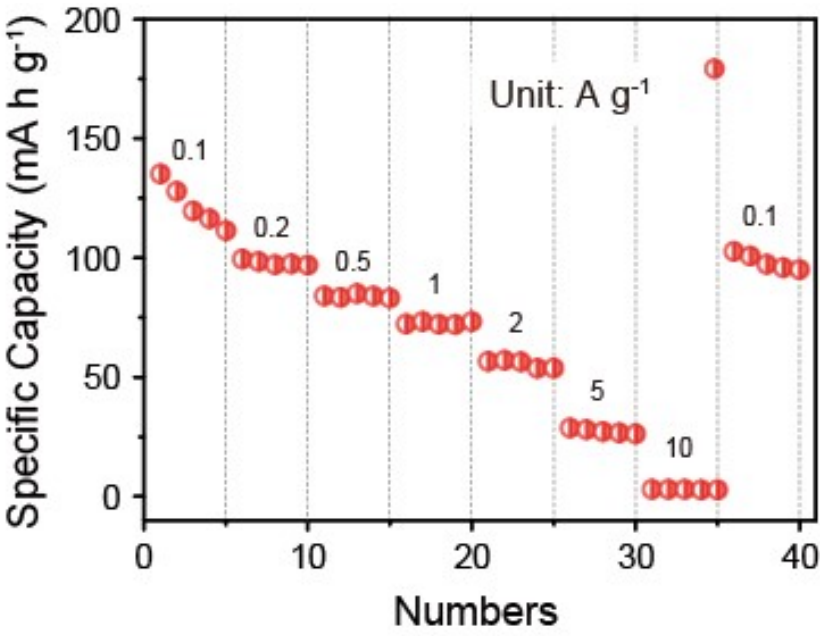

Fig. S10. Rate capability of PCC cathode at various J from 0.1 to 10 A g^{-1} in 1M $NaClO_4$/[PC+5%FEC].

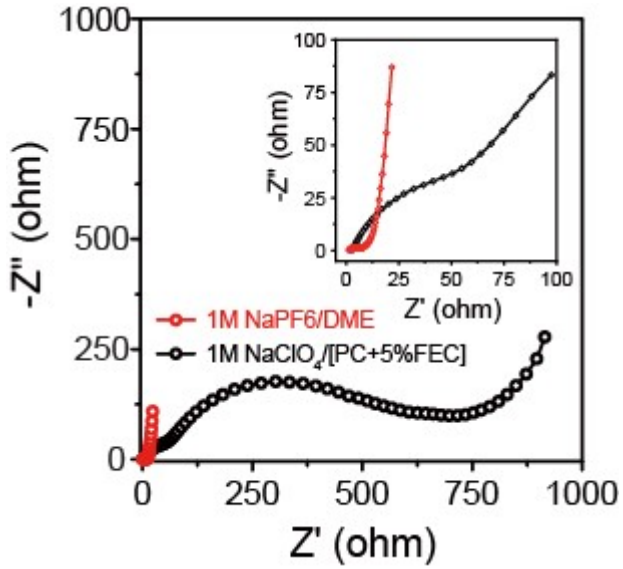

Fig. S11. Electrochemical impedance spectroscopy of PCC cathode in different electrolytes.

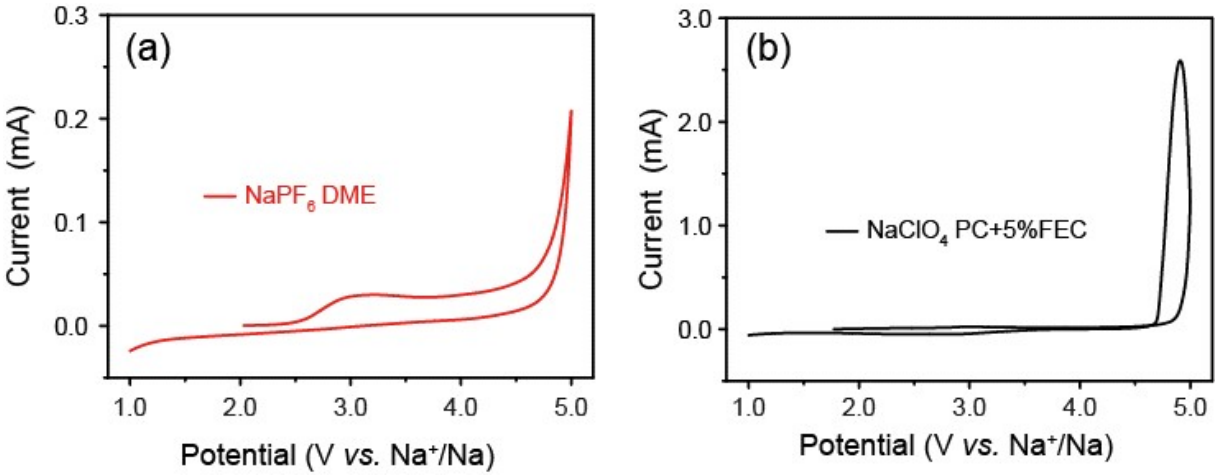

Fig. S12. The voltage window tests in different electrolytes.

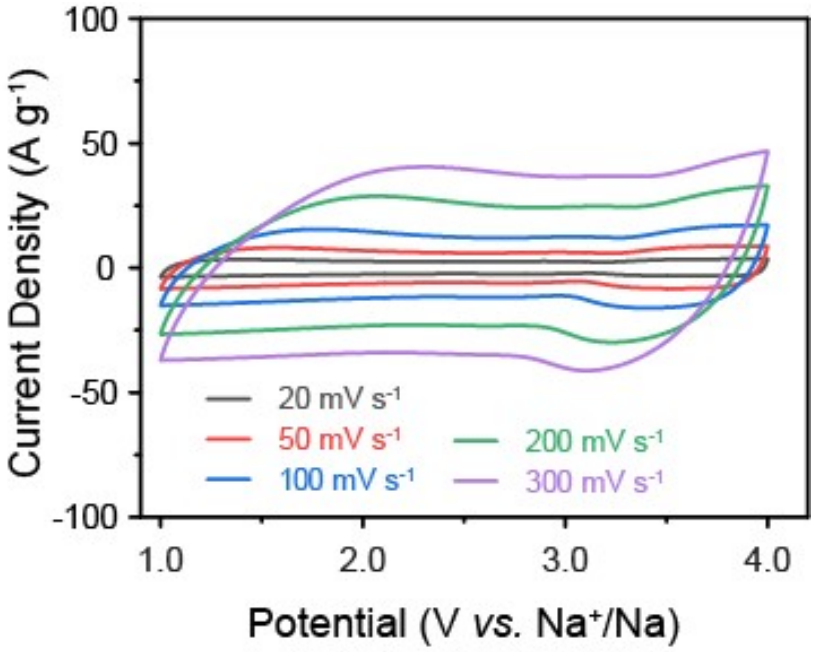

Fig. S13. CV curves of PCC cathode at varied scan rates from 20 to 300 mV s^{-1}.

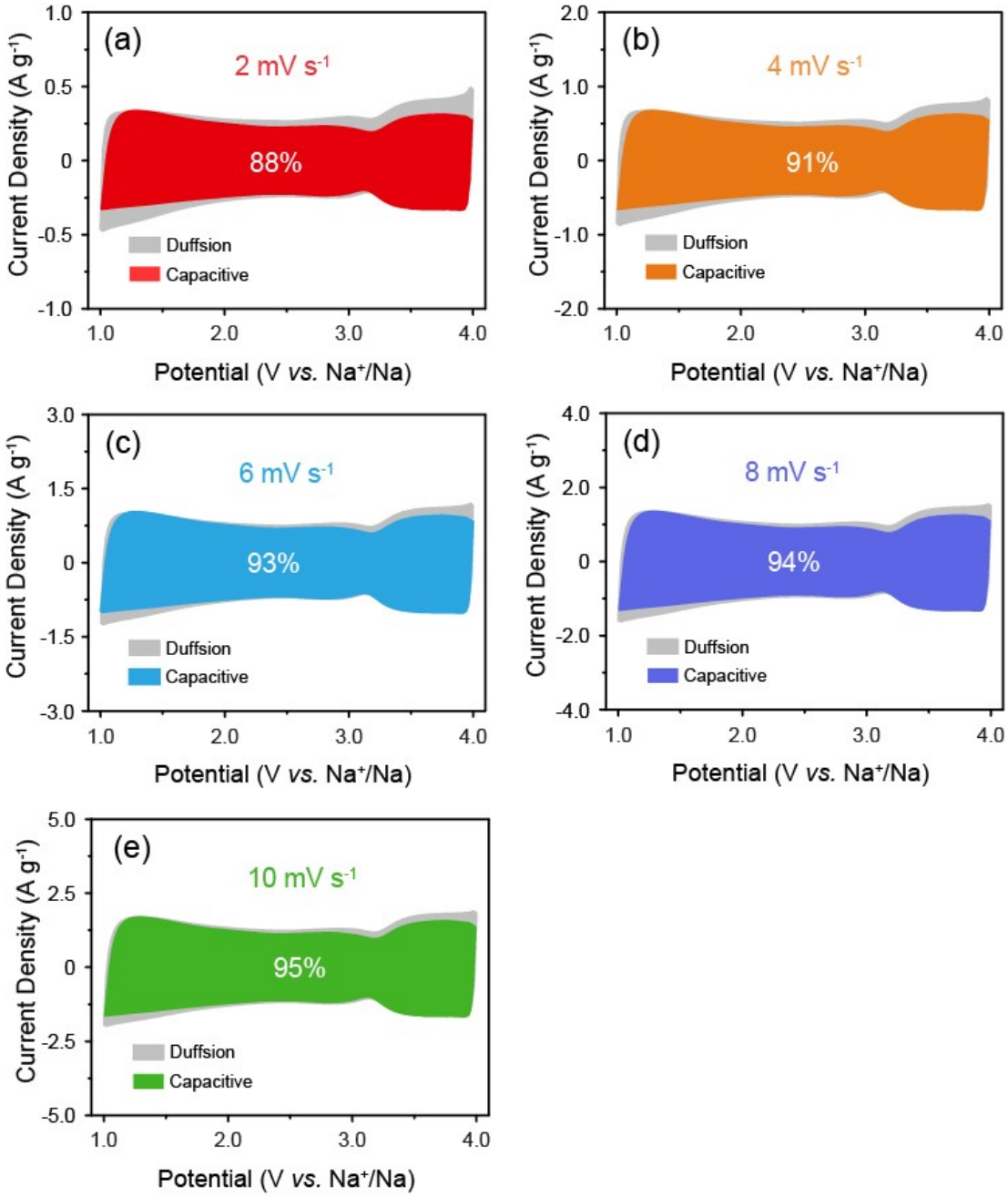

Fig. S14. CV curve of PCC cathode with the surface-controlled fraction shown by the colored region at a scan rate of (a) 2 mV s^{-1}, (b) 4 mV s^{-1}, (c) 6 mV s^{-1}, (d) 8 mV s^{-1}, and (e) 10 mV s^{-1}.

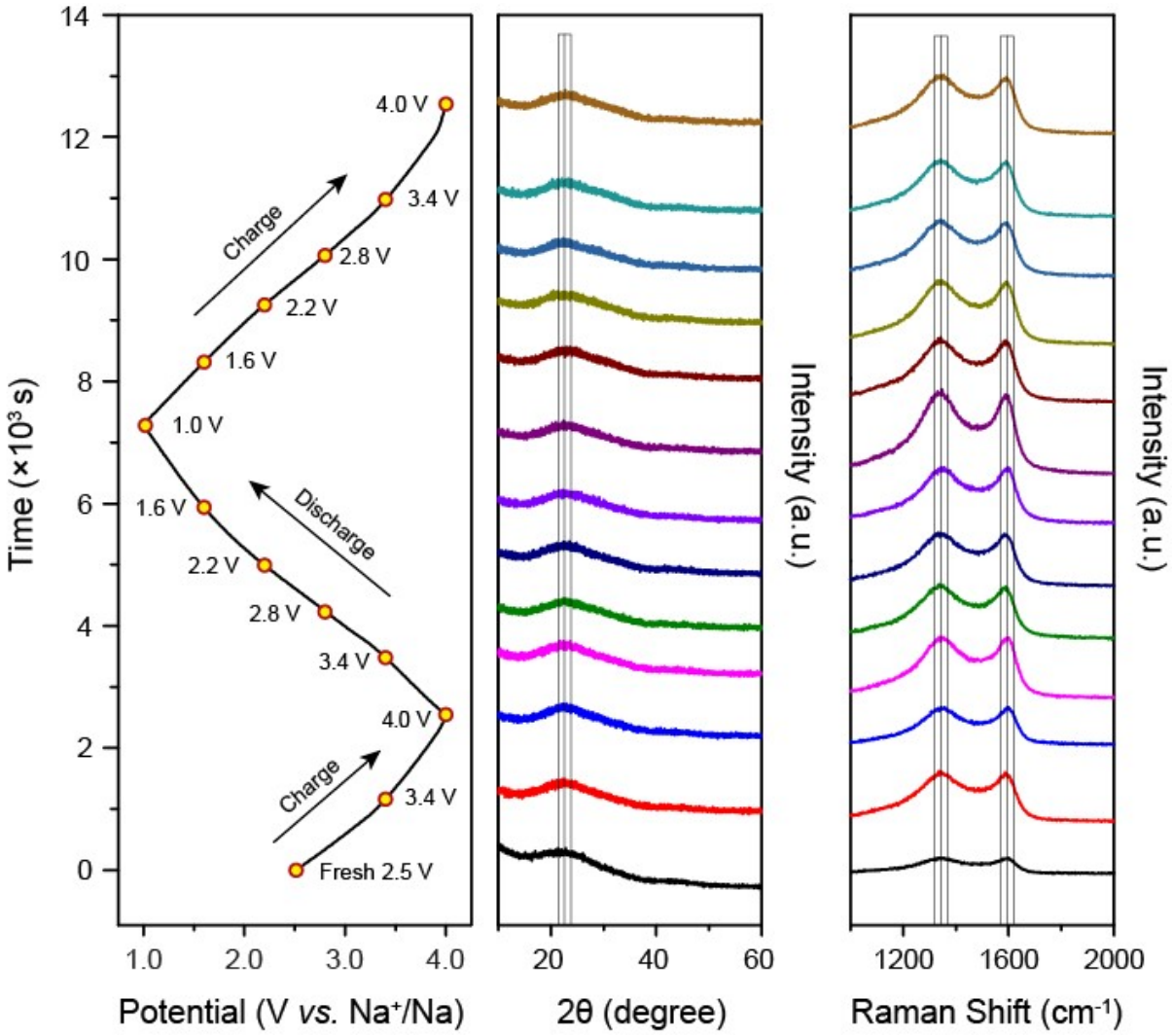

Fig. S15. Ex-situ XRD and Raman tests of PCC cathode.

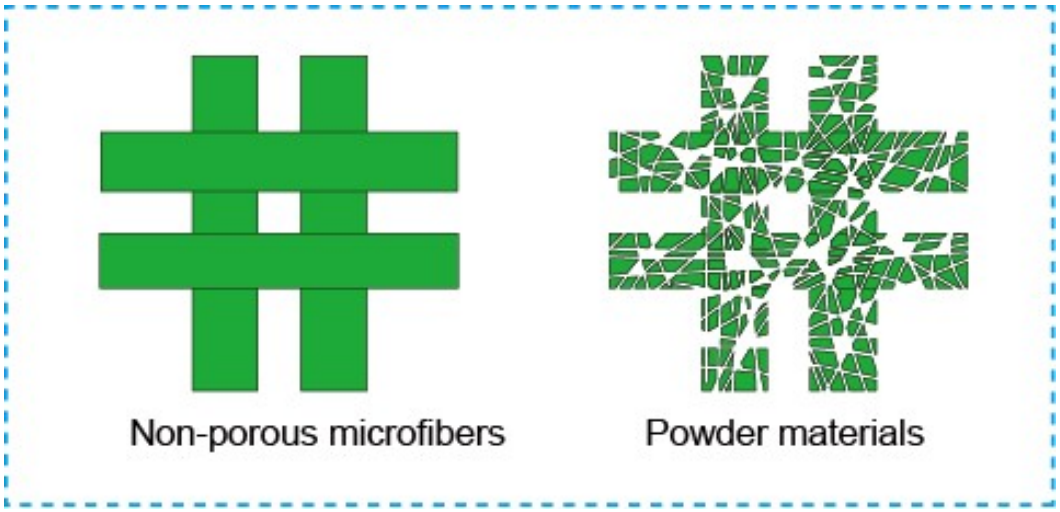

Fig. S16. Schematic illustration for the self-supporting HCC and the grated HCC powder.

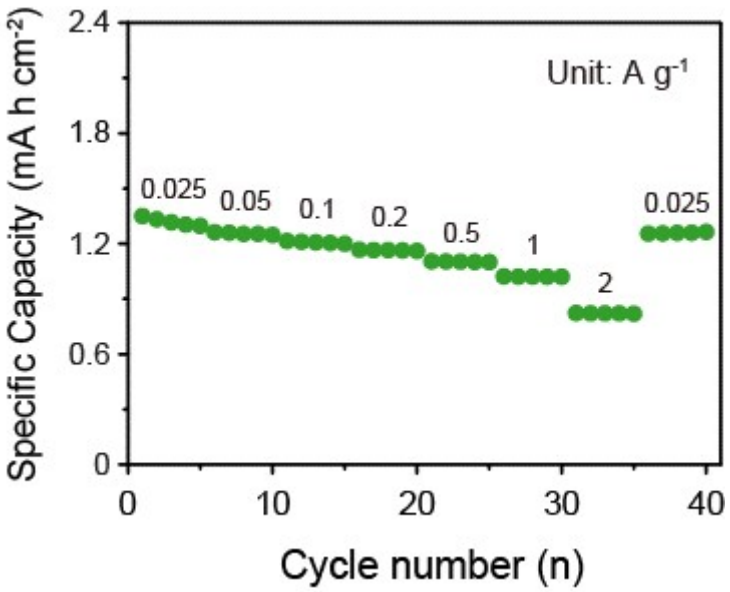

Fig. S17. Rate capability of HCC anode at various J from 0.025 to 2 A g^{-1} calculated based on area.

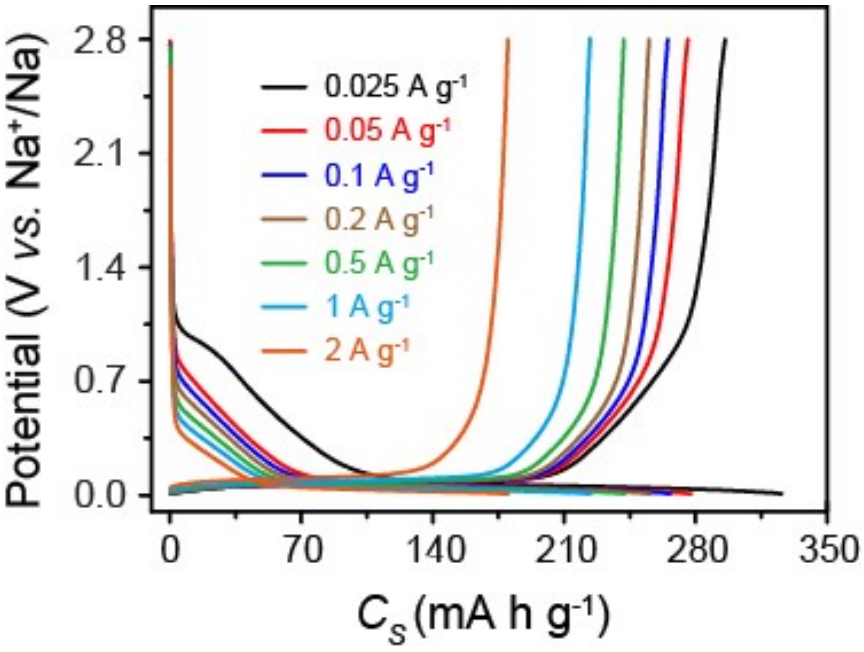

Fig. S18. GCD curves of the HCC anode at varied J.

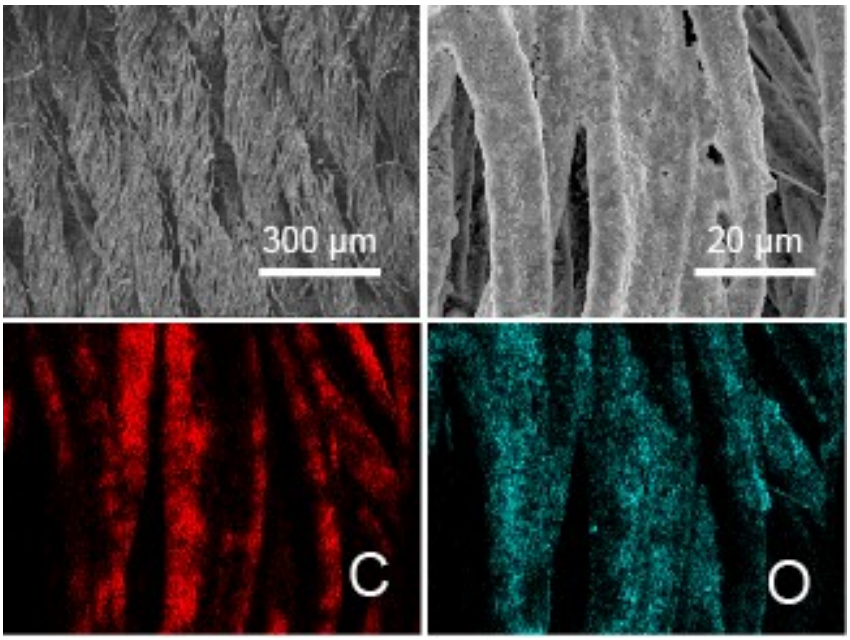

Fig. S19. SEM image and the corresponding elemental mappings of carbon and oxygen of HCC anode after 100 cycles.

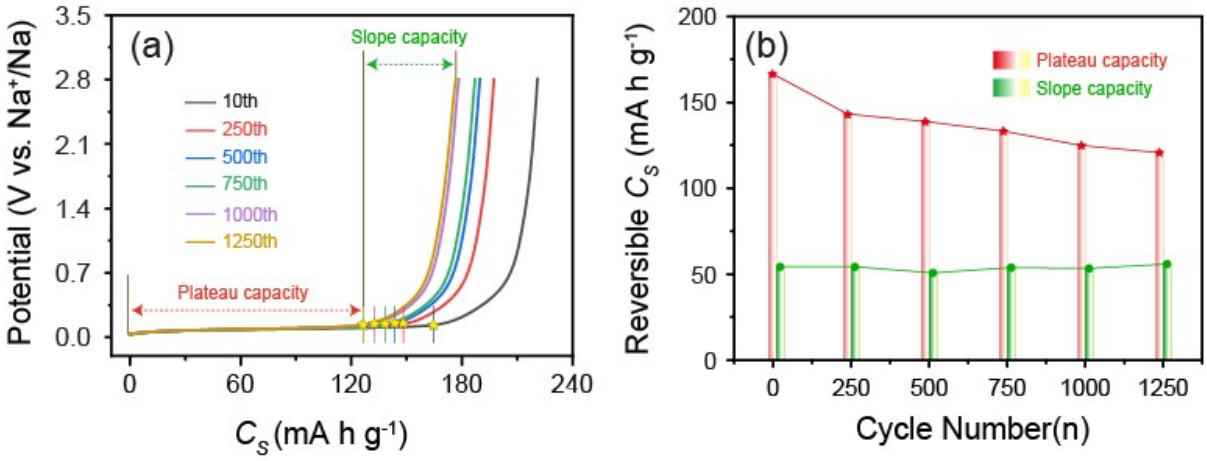

Fig. S20. (a) The charge curves of HCC anode at different cycles at 1 A g^{-1}. (b) Corresponding statistical results of plateau and slope capacity in different cycle number.

The capacity contributions of plateau and slope regions at different cycles are analysed based on the charging curves to reveal the causes of capacity degradation in HCC anode. As shown in Fig. S20, the plateau capacity exhibited a slow decline during cycling while slope capacity did not change significantly, which suggests that the capacity fading of HCC is mainly caused by gradual damage and deactivation of graphitic nanodomain during cycling.

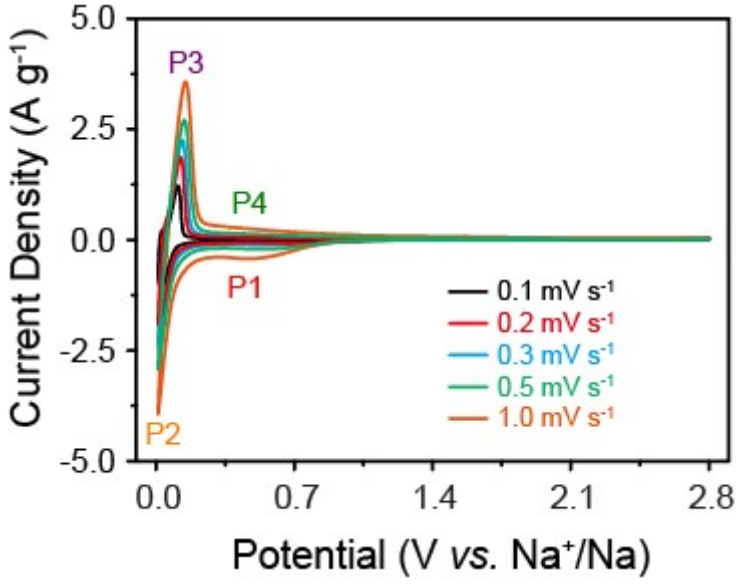

Fig. S21. CV curves of HCC anode at various scan rates in the potential range of 0.01-2.8 V.

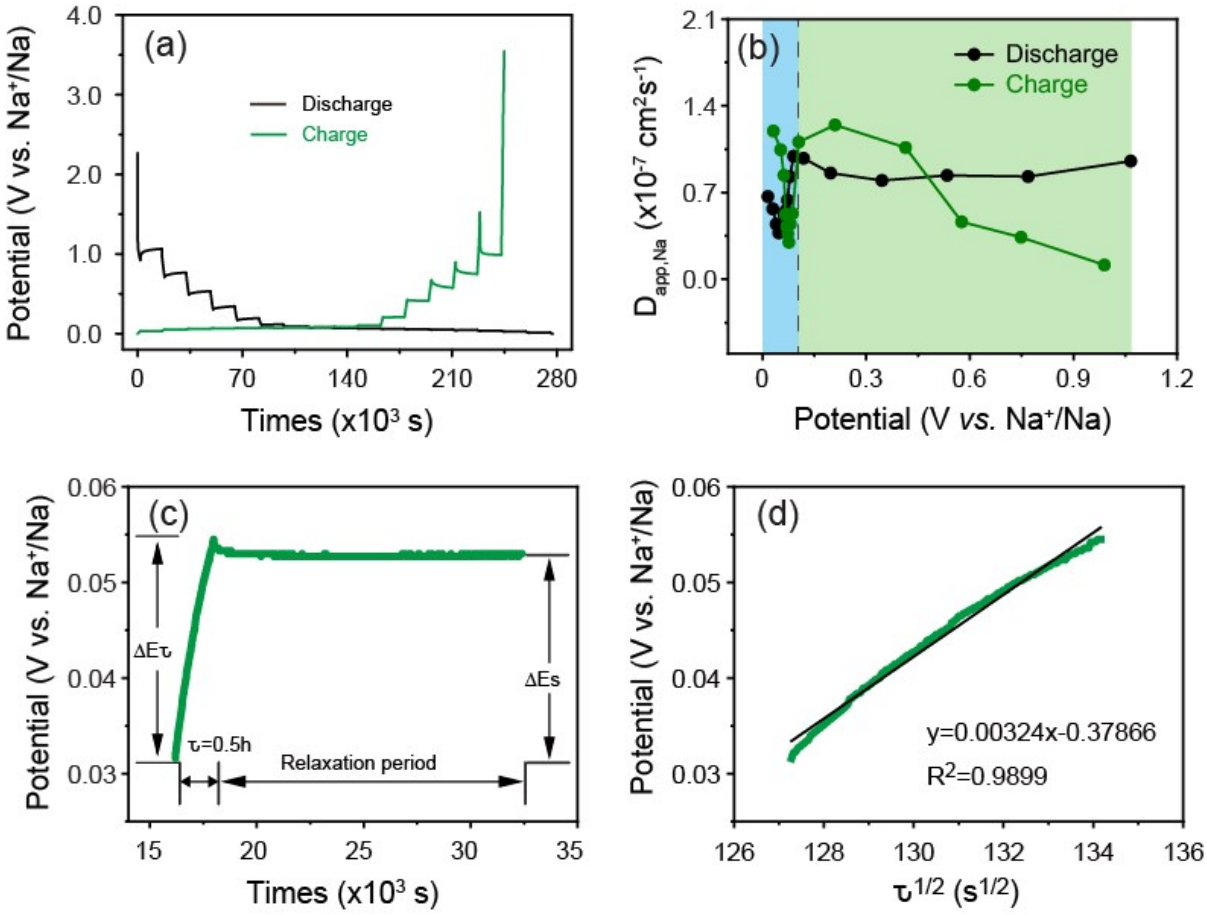

Fig. S22. (a) GITT curves of the second discharge-charge process between 0.01 and 2.8 V for HCC anode. (J = 0.04 A g^{-1}, time interval τ = 0.5 h). (b) The $D_{Na,app}$ calculated by GITT. (c) τ versus E profile for a single GITT titration. (d) linear behavior of E versus $\tau^{1/2}$.

Discussion on the GITT for the HCC:

The GITT tests were carried out to evaluate apparent Na^+ diffusion in HCC anode. Fig. S22a, b shows the GITT curves of HCC anode during the second discharge-charge process and the corresponding apparent diffusion coefficient of Na^+ in every pulse duration of 0.5 h. The D_{Na^+} values can be calculated based on the following equation S1, and the parameters needed are obtained from the potential-time curve (Fig. S22c, d):

$$D_{Na^+} = \frac{4}{\pi\tau}\left(\frac{m_B V_M}{M_B S}\right)^2\left(\frac{\Delta E_s}{\Delta E_\tau}\right)^2 \qquad \left(\tau \ll L^2/D_{Na^+}\right) \qquad \text{S1}$$

Where m_B, M_B and V_M is the mass, molecular weight, and molar volume of HCC, anode respectively; τ is the time for an applied galvanostatic current; S is the active surface of the electrode; L is the average radius of the material particles; and ΔEs and $\Delta E\tau$ are the quasi-equilibrium potential and the change of cell voltage E during the current pulse, respectively.

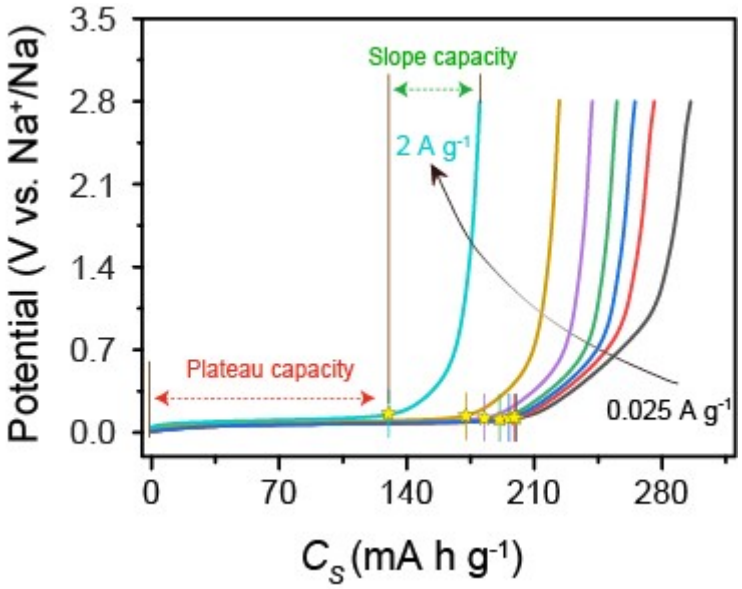

Fig. S23. (a) The charge curves of HCC anode at varied J from 0.025 to 2 A g^{-1}.

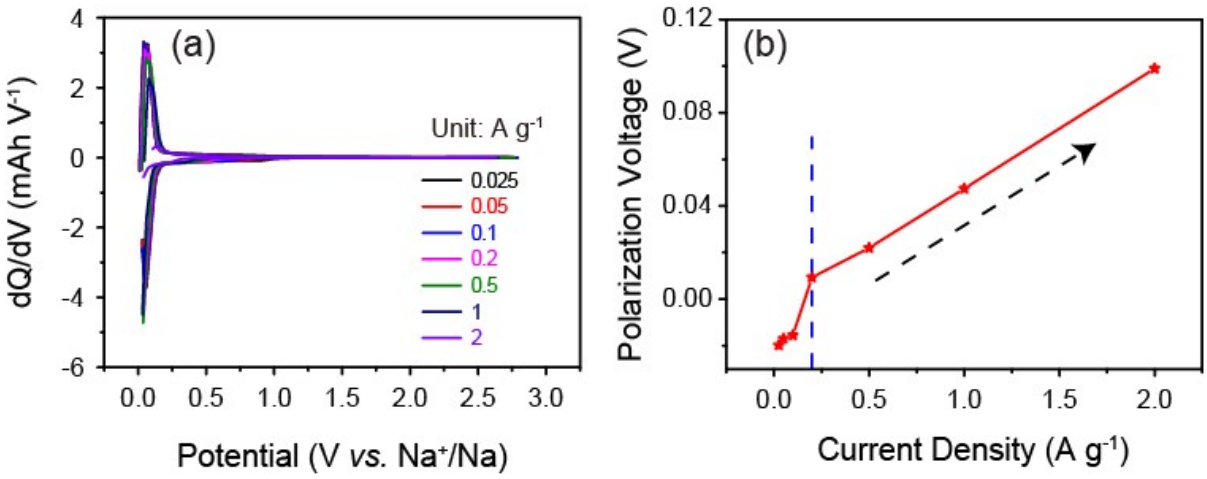

Fig. S24. (a) The dQ/dV curves of HCC anode at varied J from 0.025 to 2 A g^{-1}. (b) Corresponding polarization voltage at different J from 0.025 to 2 A g^{-1}.

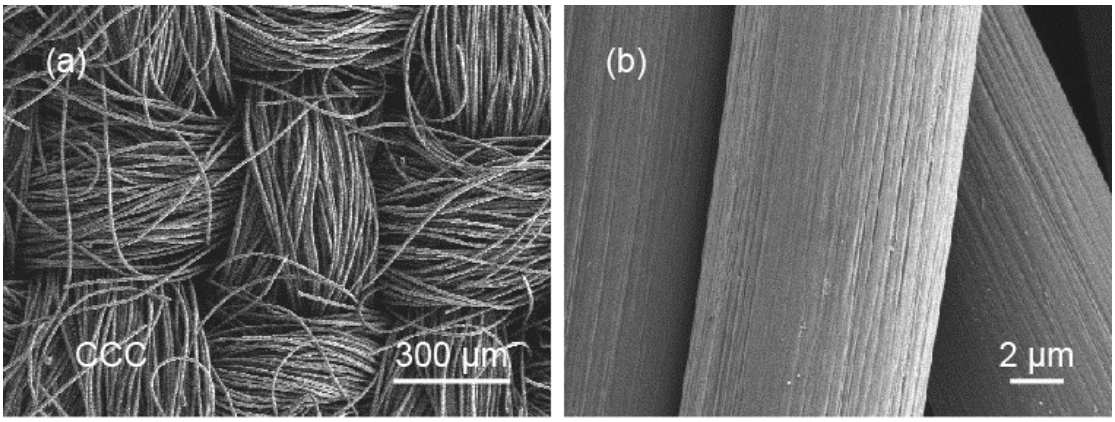

Fig. S25. SEM images of CCC.

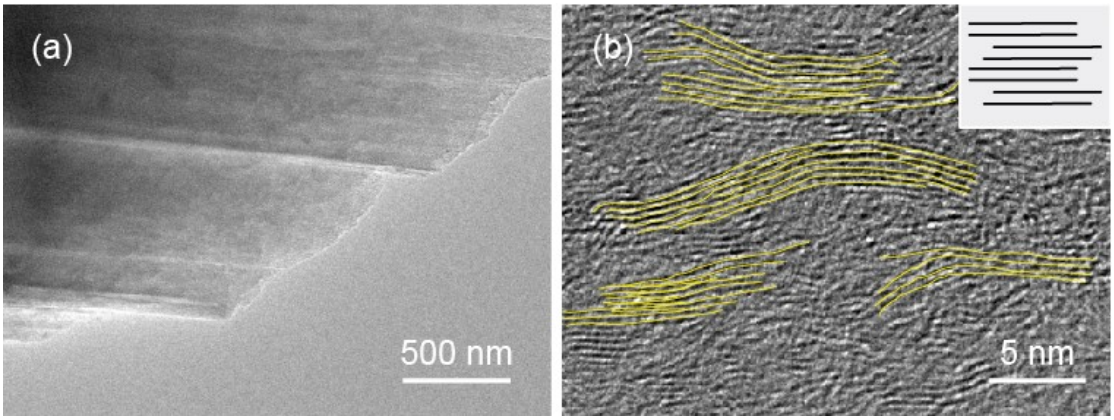

Fig. S26. (a) TEM and (b) HRTEM images of CCC.

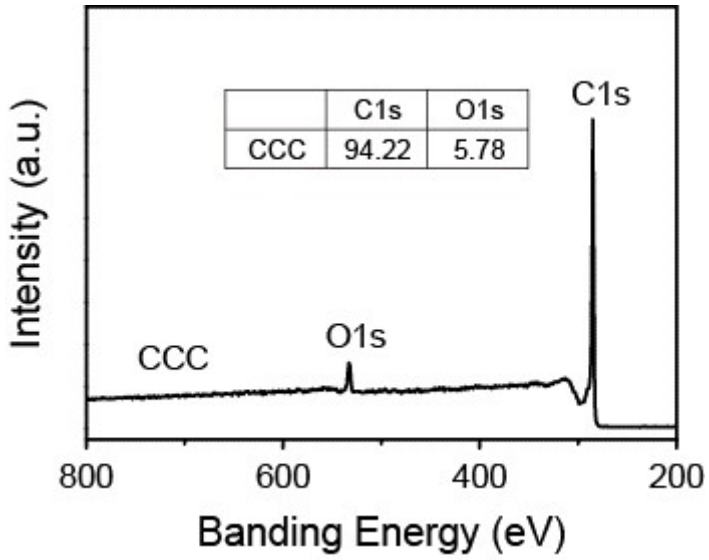

Fig. S27. XPS full spectra of CCC.

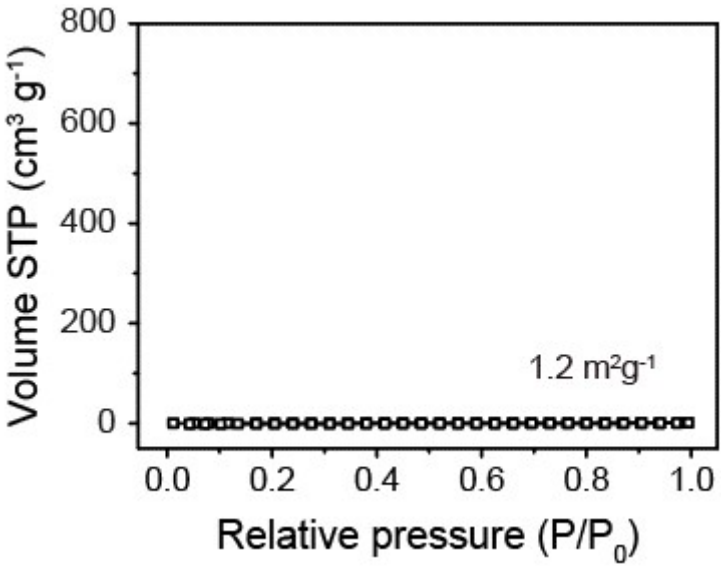

Fig. S28. N_2 adsorption/desorption isotherms of CCC.

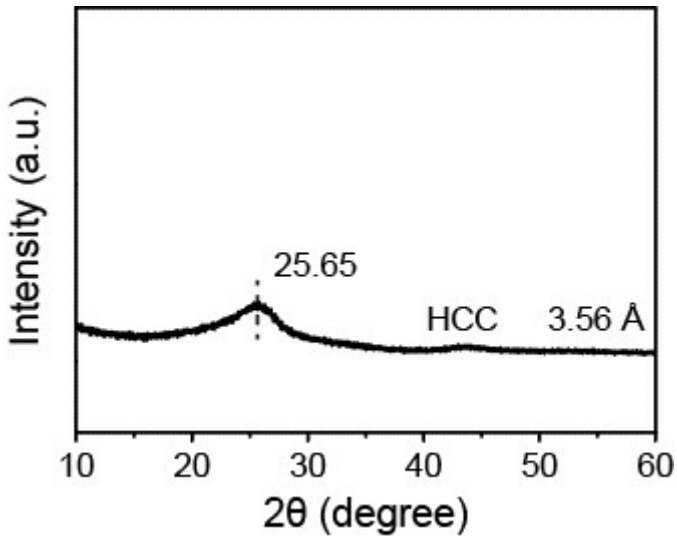

Fig. S29. XRD pattern of CCC.

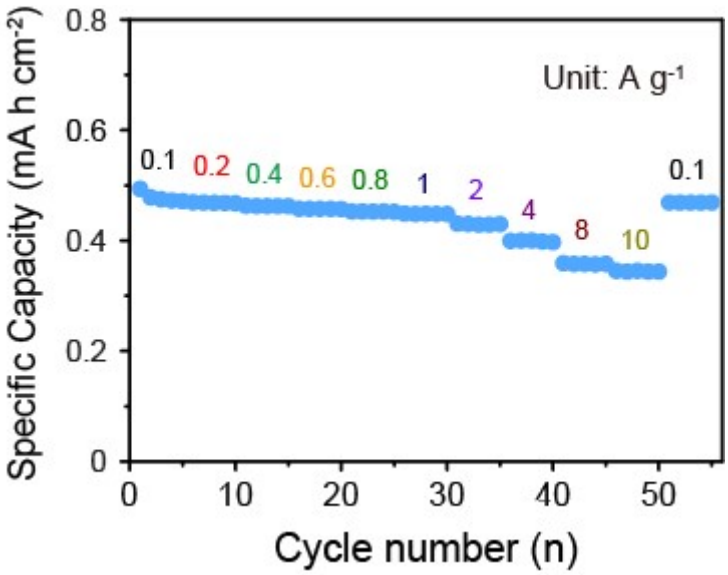

Fig. S30. Rate capability of ACSIC at various J from 0.1 to 10 A g^{-1} calculated based on area.

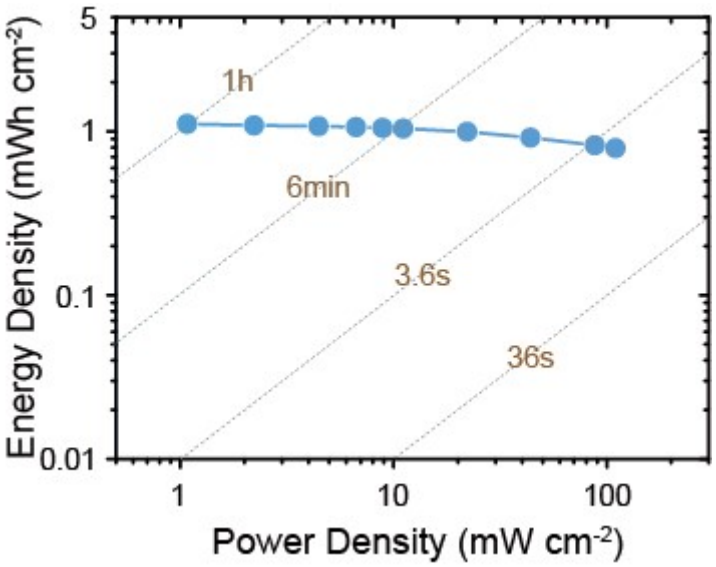

Fig. S31. Energy-power density of ACSIC calculated based on area.

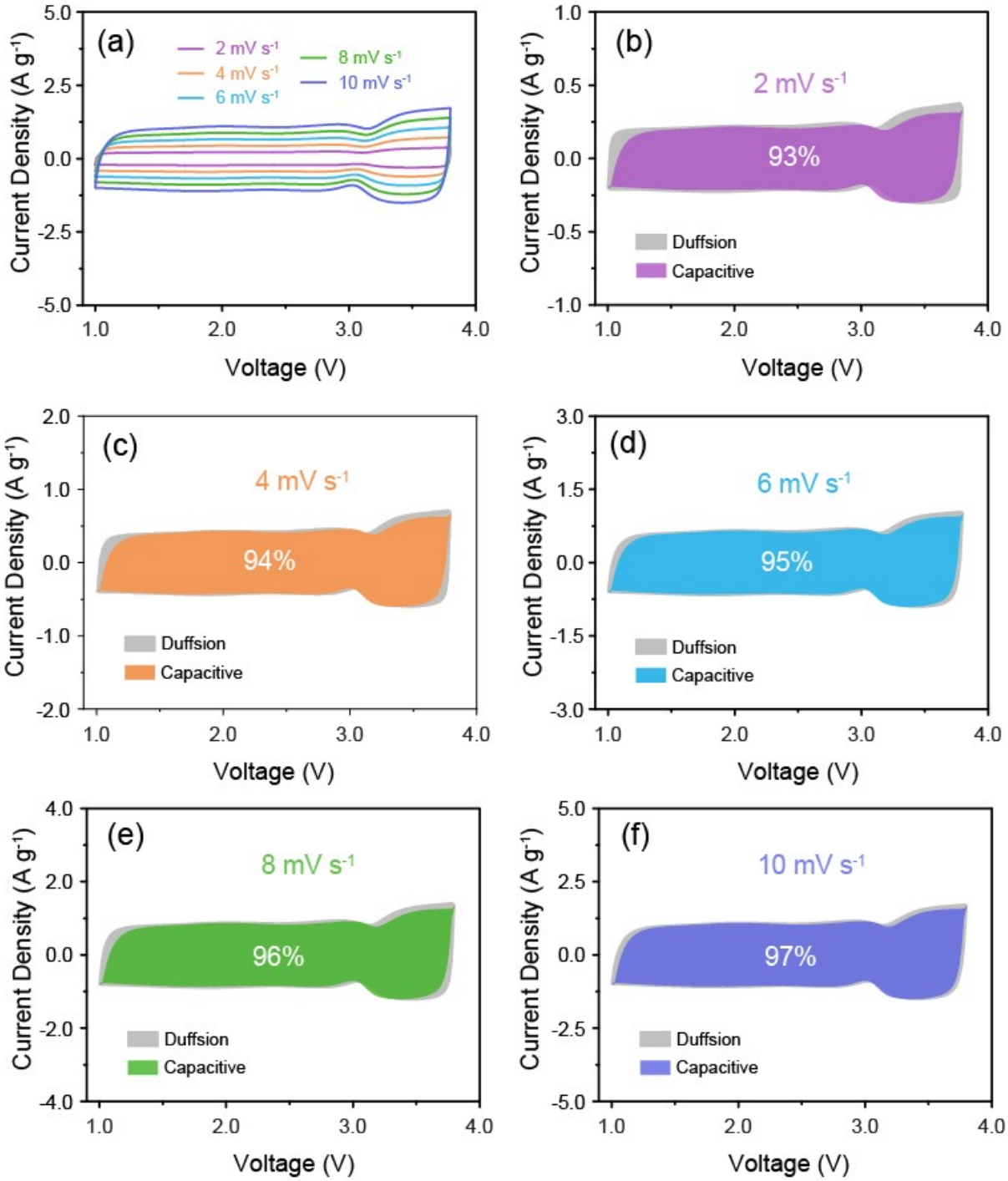

Fig. S32. (a) CV curves of ACSIC at varied scan rates from 2 to 10 mV s^{-1}. CV curve of ACSIC with the surface-controlled fraction shown by the colored region at a scan rate of (b) 2 mV s^{-1}, (c) 4 mV s^{-1}, (d) 6 mV s^{-1}, (e) 8 mV s^{-1}, and (f) 10 mV s^{-1}.

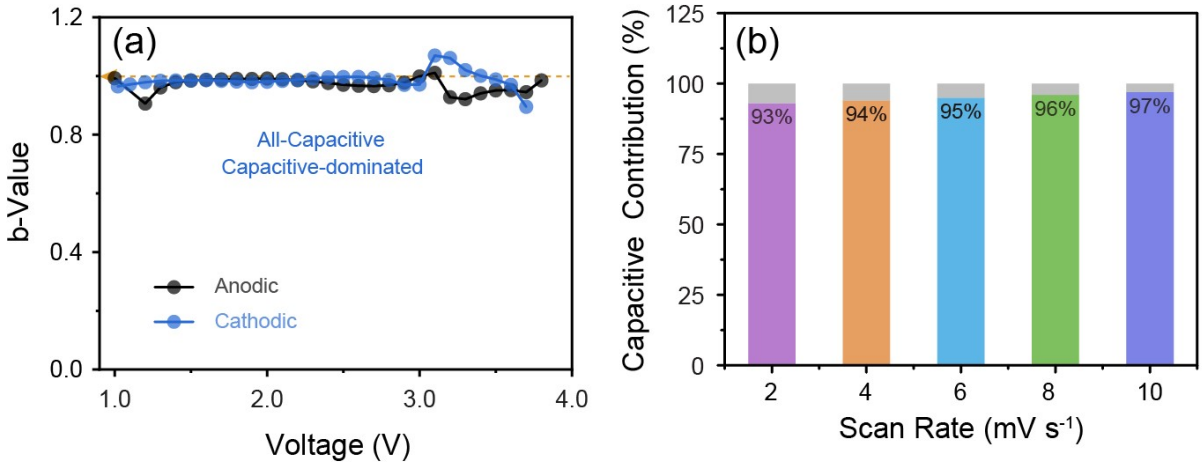

Fig. S33. (a) The b-values of ACSIC at different measured potentials. (b) Calculated contribution proportions of the surface- and diffusion-controlled processes at 2 to 10 mV s^{-1}.